THE JOURNAL OF PHYSICAL CHEMISTRY C

Article

pubs.acs.org/JPCC

Study of the Interaction between Gold Nanoparticles and Rose Bengal Fluorophores with Silica Spacers by Time-Resolved Fluorescence Spectroscopy

Hsing-Hui Lin and I-Chia Chen*

Department of Chemistry, National Tsing Hua University Hsinchu, Taiwan 30013, Republic of China

Supporting Information

ABSTRACT: The interaction between gold nanoparticles (GNPs) with silica shell as spacer, Au@SiO_2 NPs, and fluorophore rose bengal (RB) is studied using time-resolved spectroscopy. Varied sizes of GNPs with controlled thickness of silica shell were synthesized to investigate the effects on metal-enhanced fluorescence. Fluorophore RB covalently connected to prefunctionlized silica surface has spectral overlap with the plasmon resonance of the gold nanoparticle. The enhancement factor for fluorescence displaying a maximum at spacer separation ~10 nm is 2.4, 3.8, 4.6, and 5.5 for diameters 45, 65, 80, and 100 nm Au@SiO_2 NPs, respectively. Biexponential decay of emission is observed for small thicknesses of spacer, indicating multiple pathways for relaxation of the excited states. Both time constants τ_1 and τ_2 are consistently increased with increased separation of the silica spacer. The fast component has the most amplitude at short spacer thicknesses and large NP sizes. The biexponential decay is explained by the back energy transfer of the bright modes of GNPs to fluorophore being nonnegligible. For 100 nm GNPs, we find that the rate constant for energy transfer from RB to GNP is 9×10^6 to 2.0×10^{10} s^{-1} (bright + dark modes) for separation 5−45 nm, displaying a dependence on the separation of the silica shell d^{-n} with $n \approx 2.5$. The backward rate constant is 3.5×10^9 to 4.9×10^9 s^{-1} for separation 5−18 nm.

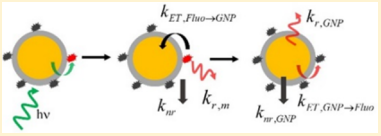

1. INTRODUCTION

Fluorescence is a methodology with zero background and high-sensitivity commonly employed in biology and medicine.[1,2] For fluorophore molecules with a low quantum yield of emission or those used as a detecting target in the presence of an interfering background, it is necessary to amplify the fluorescent intensity to achieve superior sensitivity. Fluorescence amplification by metal nanoparticles is a relatively new technology that has attracted attention recently. There are many studies on the effects and applications of fluorophores with metal nanoparticles in close proximity.[3] A review article by Lakowicz provides detailed descriptions of the effects of metal-enhanced fluorescence (MEF) and its applications.[4] A general review on theory can be found in articles by Klimov et al.[5] and Fort and Gresillon.[6] As a consequence of MEF, increased fluorescence quantum yield, decreased fluorescence lifetime, and sometimes increased molecular photostability are generally observed.[7] The local electric field on a metal nanoparticle induced by incident light enhances the excitation on the fluorophore, thereby enhancing the fluorescence. When the fluorophore lies close, the nanoparticle offers an additional nonradiative decay channel that tends to quench emission.[8,9] Consequently, the overall fluorescence intensity is varied depending on the distance of the fluorophore to the surface of the nanoparticle.[10−13]

When a fluorophore is excited by incident light or the electric field of metal nanoparticles, the excited fluorophore may induce a mirror dipole on the metal nanoparticle. The induced mirror dipole radiates highly efficient. Geddes and co-workers proposed that the MEF results primarily from the excited molecules coupling with the scattering mode of nanoparticles.[14−16] The extinction of a molecule to radiation consists of absorption and scattering portions. For small nanoparticles, the extinction is dominated by absorption, and for large nanoparticles, by scattering. Hence, large nanoparticles are likely to be more efficient for MEF. Indeed, some studies have reported that the enhancement of fluorescence increases with the size of metal nanoparticles.[17]

The damping processes of nanoparticle plasmons consist of radiative and nonradiative pathways. The excited fluorophore can transfer energy to a nearby metal nanoparticle to create surface plasmon modes. If the excited fluorophore is coupled to the dipole mode of the nanoparticle, the plasmons decay both radiatively and nonradiatively; if it is coupled to the high-order modes, they dissipate energy only nonradiatively.[18] Many theoretical and experimental studies have reported on the energy transfer rate from a fluorophore to a metal nanoparticle leading to fluorescence quenching.[19−21] Fluorescence resonance energy transfer (FRET) theory, which considers the dipolar interaction of donor and acceptor, has limitations because FRET physically originates from the weak electromagnetic coupling of two point dipoles.[22] Several theoretical studies have reported that the energy transfer from a fluorophore to a metal nanoparticle is attributed to nanosurface energy transfer (NSET) and should follow d^{-4} dependence, d denoting the distance from the fluorophore to the surface.[23] NSET is generally applied to nanoparticles of diameter <10

Received: August 31, 2015
Revised: November 6, 2015
Published: November 6, 2015

DOI: 10.1021/acs.jpcc.5b08477
J. Phys. Chem. C 2015, 119, 26663−26671

Scheme 1. Attachment of Rose Bengal on GNPs

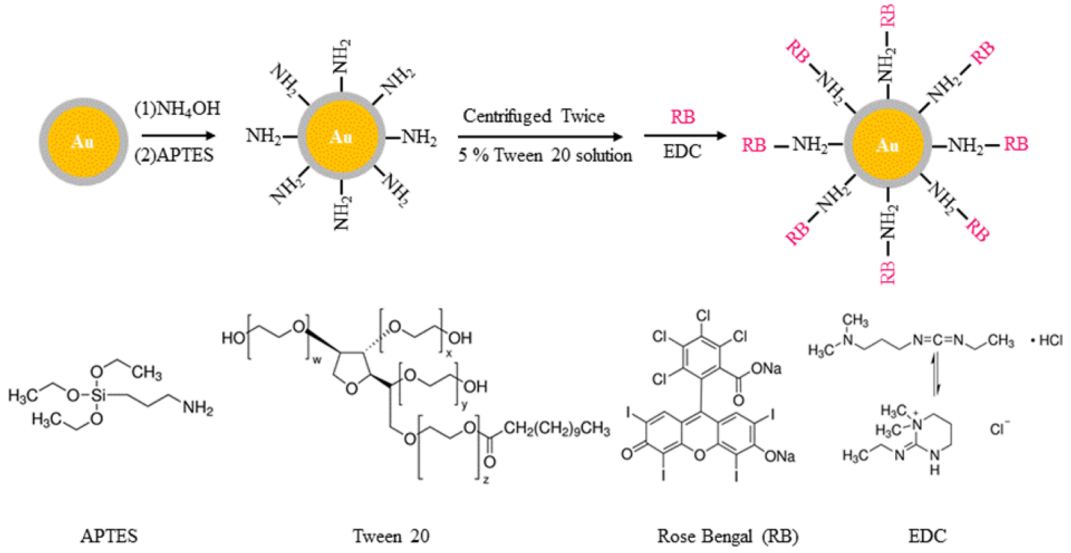

nm[24,25] and is found to deviate from the experimental data for nanoparticles of 10 nm diameter.[26−28] However, a more recent experimental study reveals that the distance dependence is related to the size of the nanoparticles and that the exponent of dependence is less than 4 for larger nanoparticles.[26]

MEF also depends on the shape of the nanoparticles,[29] the distance from the fluorophore molecule to the surface of nanoparticles,[30,31] and the spectral overlap of the emission of fluorophore with the absorption of the nanoparticle.[32−34] In the present work, we synthesized nanoparticles of varied sizes and coated them with silica shells (Au@SiO_2 NPs) of controlled thickness. A silica shell offers chemical inertness, electronic insulation, and robustness, and it can be synthesized cheaply, so silica shells were used as spacers for varying the distance between the fluorophores and gold nanoparticles (GNPs). Fluorescence enhancement is known to critically depend on the enhanced excitation and radiative decay rate. The overlap between absorption/emission band of rose bengal (RB) and plasmonic band of GNP could lead to significant fluorescence enhancement. We employed time-resolved fluorescence spectroscopy to study the size and distance effects on MEF. The decay behavior is sensitive to the interaction between the fluorophore and nanoparticle and it is expected to provide detailed information on the coupling mechanism. On the basis of experimental data, we construct suitable theoretical models to explain the interaction between the GNPs and fluorophores.

2. EXPERIMENTS

2.1. Materials. Gold(III) chloride trihydrate ($HAuCl_4 \cdot 3H_2O$) was purchased from Alfa Aesar. Sodium citrate, cetyltrimethylammonium bromide (CTAB), tetraethyl orthosilicate (TEOS), poly(sodium 4-styrenesulfonate) (PSS), sodium chloride (NaCl), poly(allylamine hydrochloride) (PAH), polyvinylpyrrolidone (PVP), 2-propanol, rose bengal (RB), 1-ethyl-3-(3-(dimethylamino)propyl)carbodiimide HCl (EDC), ammonium hydroxide solution (NH_4OH), (3-aminopropyl)-trimethoxysilane (APTES), and polyoxyethylene (20) sorbitan monolaurate (Tween 20) were from Sigma-Aldrich. All chemicals were used as received. Pure deionized water (Milli-Q Millipore, 18.2 MΩ/cm) was used in all preparations.

2.2. Synthesis of Gold Nanoparticles (GNPs). Highly monodispersed large size spherical GNPs were synthesized using the seeded growth method. Typically, 0.1 g of sodium citrate was added to 50 mL of 2.5×10^{-4} M $HAuCl_4 \cdot 3H_2O$ at 80 °C under vigorous stirring. The gold seed solution was reacted for a few minutes and then was centrifuged before use. The first growth step was carried out by adding 150 μL of 0.1 M ascorbic acid to a solution containing 300 μL of 0.025 M $HAuCl_4 \cdot 3H_2O$ and 26.6 mL of 0.05 M CTAB at 35 °C, followed by the addition of 3 mL of seed solution. Greater sizes of GNPs were grown by addition of the first growth GNPs. Varied GNPs sizes were obtained by varying portions of the seed solution.

2.3. Silica-Coated GNPs. The homogeneous silica coating was based on a combination of the polyelectrolyte layer-by-layer assembly and the hydrolysis and condensation of tetraethylorthosilicate (TEOS).[35] Typically, 300 mL of synthesized GNPs were centrifuged twice and redispersed in 100 mL of deionized water. A 100 mL aliquot of negatively charged PSS solution (2 mg/mL, 6 mM NaCl), first sonicated for 30 min, was adsorbed on positively charged CTAB-capped GNPs, and reacted for 3 h. The PSS-modified NPs were centrifuged twice to remove excess PSS and then were added to 100 mL of PAH solution (2 mg/mL, 6 mM NaCl). This PAH solution was centrifuged to remove the unreacted PAH. About 100 mL of PSS/PAH functionalized GNPs ([Au] = 7.6×10^{-4} M) was added to a PVP solution to cover the NPs with ca. 80 PVP molecules/nm. The mixture was stirred for 12 h, centrifuged to remove excess polymers, and redispersed in 108 mL of 2-propanol. About 2 mL of deionized water was added to 12 mL of PVP-coated nanoparticles and allowed to proceed for 20 min. Then TEOS in 2-propanol was added, followed by the addition of 200 μL of NH_4OH. The mixture was allowed to react for 2 h.[36] Silica shells of varied thickness were obtained by controlled TEOS addition. Silica NPs without GNPs were synthesized using the identical method. The size of silica NPs is 105 ± 5 nm, and its TEM image is shown in Supporting Information Figure S4.

2.4. Rose Bengal-Coated Silica GNPs. The covalent attachment of RB to the silica surface was performed through conjugation between the carboxylic groups (COO^-) of RB and

DOI: 10.1021/acs.jpcc.5b08477
J. Phys. Chem. C 2015, 119, 26663−26671

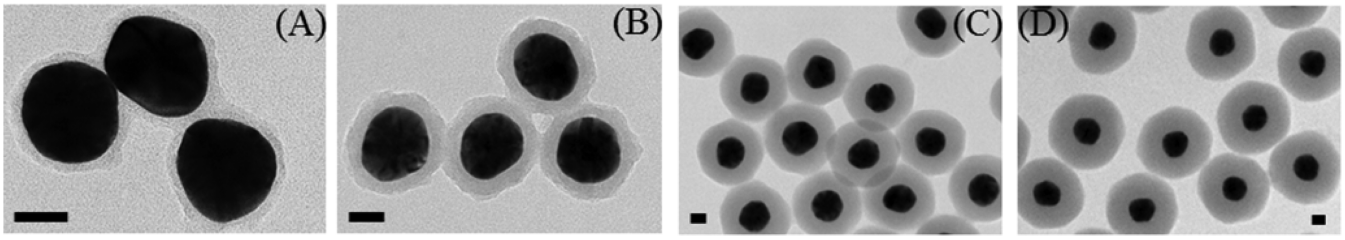

Figure 1. Representative TEM images of Au@SiO_2 NPs (core diameter = 45 ± 3 nm) with various silica shell thicknesses: 5 (A), 10 (B), 30 (C), and 40 nm (D). The scale bar is 25 nm.

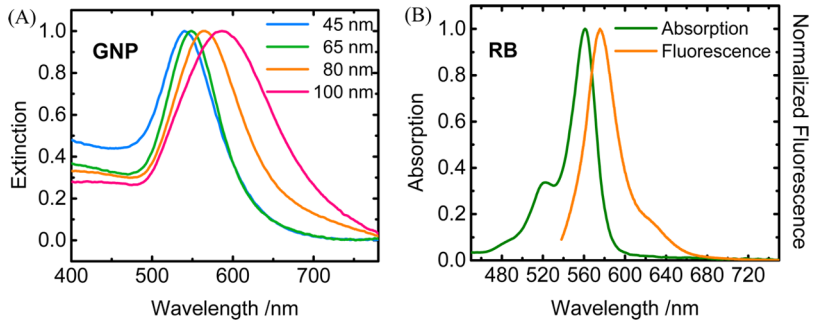

Figure 2. (A) Extinction curves of gold nanoparticles with diameters of 45, 65, 80, and 100 nm. The peak positions of the surface plasmon resonance were 540, 549, 563, and 587 nm, respectively. (B) Steady-state spectra of RB in 2-propanol with maximal absorbance/fluorescence at 561/575 nm.

the amine groups (−NH_2) prefunctionalized on the silica surface. Au@SiO_2 NPs were dispersed in 2-propanol, then NH_4OH was added and the mixture stirred for 20 min. Amine-functionalized silica NPs were carried out by adsorption of APTES, and reaction continued for 2 h.[37] After functionalization, the nonionic surfactant Tween 20 was used to increase the colloidal stability for positively charged NPs. About 20 μL of 5 × 10^{-5} M RB solution was added to 10 mL of 2-propanol, followed by EDC. The RB−EDC conjugation reaction proceeded for 20 min. The Au@SiO_2−NH_2 NPs were washed twice. Subsequently, 60 μL RB−EDC solution was mixed with 3 mL of Au@SiO_2−NH_2 NPs dispersion (0.01−0.1 nM) for 3 h at room temperature. The excess RB was removed by three cycles of centrifugation. The unreacted RB was collected to estimate the amount of RB deposited on the Au@SiO_2−NH_2 NPs. To prevent the dye−dye interaction and the formation of aggregates, the concentrations of RB were kept low to maintain dye−dye separation of greater than 15 nm on the surfaces of the NPs. The overall synthetic procedure for attachment of RB onto GNP is depicted in Scheme 1.

2.5. Characterization. Absorption spectra were taken using a Hitachi U-3900H UV/vis spectrometer to determine the surface plasmon maxima and GNP concentration. The scanning electron microscopy (SEM) images were obtained on a scanning electron microscope (JSM-7000F). For thin silica shells, the high resolution transmission electron microscopy (TEM) imaging was performed on an electron microscope (JEM-2100). Because a small amount of RB was deposited on the Au@SiO_2−NH_2 NPs, we developed a self-designed fluorescence spectrometer to obtain the emission curves. A continuous wave (cw) 532 nm laser (Photop Suwtech, DPGL-2100F) served as the excitation light source; the fluorescence signal passed through a notch filter, and a monochromator (iHR550, Jobin Yvon) was detected with a liquid nitrogen cooled CCD detector (Jobin Yvon).

Time-resolved fluorescence measurements were carried out by time-correlated single-photon counting (TCSPC) at the magic angle of detection in which the emission polarizer was set at 54.7° relative to polarization of the excitation pulse to remove the effect rotational correlation time of fluorophore.[38] The light source of 532 nm was the second harmonic output from a Nd:YVO_4 laser (picoTRAIN, High-Q Laser) with a pulse width of ∼10 ps and a repetition rate of 26.6 MHz. A notch filter and a long-pass filter in combination with a bandpass filter (bandwidth 10 nm) were used to minimize the scattering signals from GNPs. However, not all scattering signals could be eliminated. Au@SiO_2 NPs at the same concentration were used as a reference to obtain the background signal for removing the scattering signal from the GNPs. Fluorescence emission of 580 ± 5 nm was detected with a multichannel plate photomultiplier (MCP-PMT, Hamamatsu). After a preamplifier, the signal was sent to a TCSPC board (HydraHarp 400, PicoQuant). The setup had an instrument response function (IRF) of 30 ps at full-width at half-maximum (fwhm).

3. RESULTS AND ANALYSIS

The gold nanoparticles, Au@SiO_2 NPs, with diameters of 45 ± 3, 65 ± 4, 80 ± 7, and 100 ± 7 nm, and with silica shell thickness roughly 5, 10, 30, and 40 nm for the 45 nm NPs, and thickness 5, 10, 18, 35, and 45 nm for the diameter 65, 80, and 100 nm NPs, respectively were synthesized. The TEM images of Au@SiO_2 NPs for the 45 nm NPs are shown in Figure 1 (see the Supporting Information Figures S1−S3 for the TEM images of the other sizes). The silica shell around the metal NPs is clearly visible in these images, and no NPs with incomplete shells were found. The measured thickness and uncertainty are listed in the Supporting Information Table S1. Figure 2A displays the UV−vis absorption spectra of the PVP-coated GNPs in 2-propanol with the surface plasmon resonance band centered at 540, 549, 563, and 587 nm for the 45, 65, 80, and 100 nm GNPs, respectively. When GNPs were coated with silica, the band position has a red shift <15 nm (peak positions are displayed in Table S2 and Figure S5). Rose bengal was used

DOI: 10.1021/acs.jpcc.5b08477
J. Phys. Chem. C 2015, 119, 26663−26671

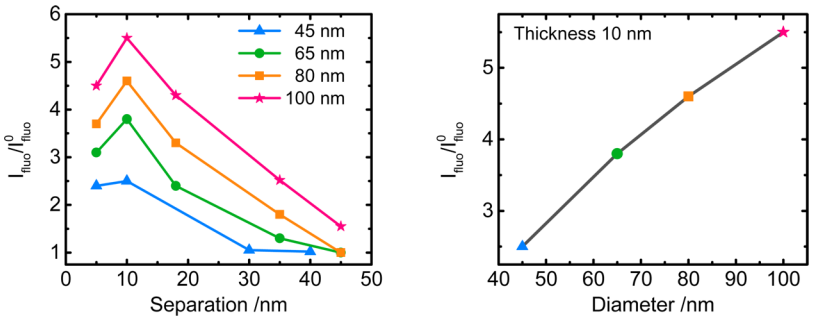

Figure 3. Fluorescence enhancement factor (uncertainty ~5%) as a function of separation with excitation wavelength 532 nm. The sizes of the gold nanoparticle were 45 (triangle), 65 (circle), 80 (square), and 100 nm (star).

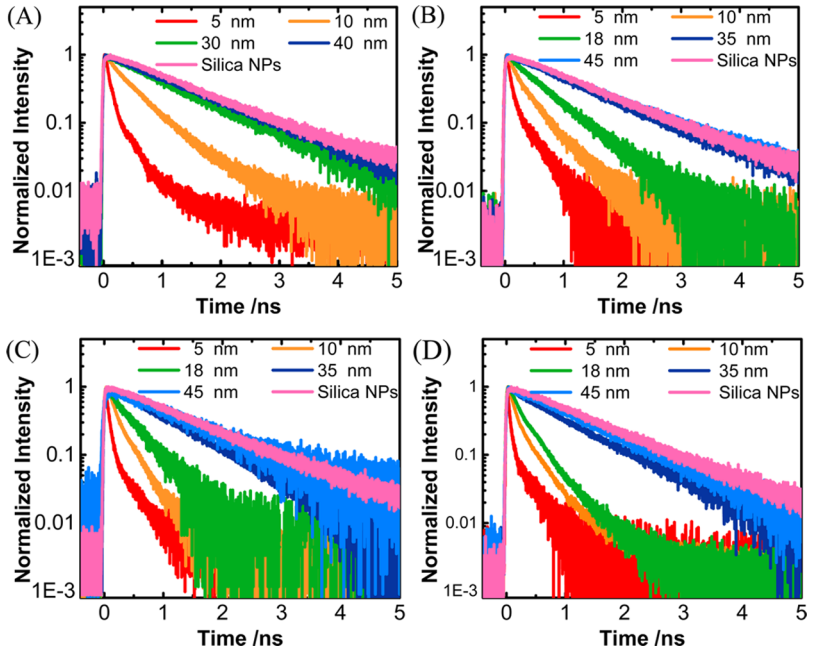

Figure 4. Fluorescence decay curves of Au@SiO_2−RB and silica−RB NPs with an excitation wavelength of 532 nm for various thicknesses of silica spacer. The diameters of gold NPs in (A)−(D) are 45, 65, 80, and 100 nm, respectively.

as the target molecule because its absorption and fluorescence bands are close to the surface plasmon resonance of GNPs, as shown in Figure 2B.

The fluorescence enhancement was obtained following the method reported by Reineck et al.[19] When the excitation light is within the surface plasmon resonance of GNPs, the excitation light can be absorbed or scattered by GNPs. The scattering loss (factor L_{scatt}) was determined by comparing the intensity of RB in 2-propanol with and without Au@SiO_2 added in solution. The fluorescence intensity, I_{sample}, of Au@SiO_2−RB NPs measured at wavelength 580 nm was corrected over the scattering loss then is normalized over the intensity of RB in 2-propanol solution $I_{RB\text{-}soln}$ at the same wavelength range and concentration.

$$I_{Fluo} = \frac{I_{sample}}{I_{RB\text{-}soln}(1 - L_{scatt})} \quad (1)$$

Silica NPs coated with RB, silica−RB NP, were used as a reference for the intrinsic fluorescence intensity. The intensity $I_{RB\text{-}silica}$ was normalized over the intensity of RB in 2-propanol $I_{RB\text{-}soln}$ at the same wavelength range and concentration to obtain I^0_{Fluo}

$$I^0_{Fluo} = I_{RB\text{-}silica}/I_{RB\text{-}soln} \quad (2)$$

The fluorescence enhancement factor, defined as I_{fluo}/I^0_{fluo}, was then calculated, and the values are displayed in Figure 3 (see the Supporting Information for the fluorescence spectra). The observed fluorescence enhancement is a combination of an increase due to enhanced excitation and induced dipole interaction and a decrease due to additional quenching from being close to the metal nanoparticle. For all sizes, the fluorescence enhancement reaches a maximum near 10 nm and decreases progressively with an increase in spacer separation. The reduction in the thinnest separation is attributed to significant quenching by the nanoparticles. The enhancement factor at 10 nm separation is 2.4, 3.8, 4.6, and 5.5 for the 45, 65, 80, and 100 nm Au@SiO_2 NPs, respectively, and increases with the size of nanoparticle.

The emission decay curves of Au@SiO_2−RB and silica−RB NPs with excitation wavelength of 532 nm are displayed in Figure 4. The decay curves of Au@SiO_2−RB at short separations displayed biexponential behavior. To verify biexponential behavior, residuals analysis is provided in the Supporting Information. The decay approaches a single exponential when RB lies away from the surfaces of

DOI: 10.1021/acs.jpcc.5b08477
J. Phys. Chem. C 2015, 119, 26663−26671

nanoparticles. Figure 5 shows the best fitted time constants vs the thickness of silica. The emission curves of both silica−RB

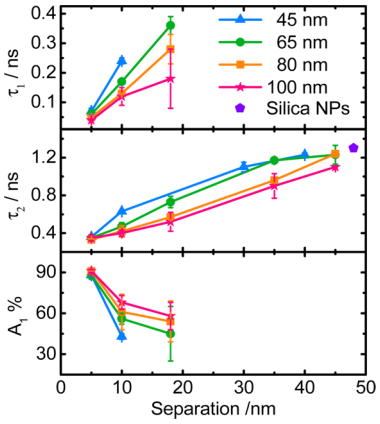

Figure 5. Fitted time constants and amplitude of the fast component A_1 vs thickness of spacer of Au@SiO_2−RB NPs with an excitation wavelength of 532 nm. The diameters of gold nanoparticles are 45 (triangle), 65 (circle), 80 (square), and 100 nm (star). The pentagon point shows the time constant of RB-decorated silica NPs.

NPs and free RB in 2-propanol solution display single exponential decay with the time constant ~1.3 ns. This also implies that no aggregation occurs between RB molecules. For Au@SiO_2−RB with a spacer thickness of ≤20 nm, the fluorescence curves feature biexponential decay. Both time constants τ_1 and τ_2 consistently increase with separation. For greater separations, the fast component disappears, and the percentage of the fast component decreases, as displayed in Figure 5. At the smallest separation, the fast component dominates and then decreases in amplitude with silica shell thickness. The portion of the fast component decreases relatively slowly for large NPs. For 45 and 65 nm GNPs with separation greater than 40 nm, the time constants are similar to that of silica NP−RB, indicating little interaction between Au NPs and RB. However, for larger GNPs, the interaction becomes greater and leads to shorter lifetime in 100 nm GNPs, even when the separation is as long as 45 nm.

4. THEORETICAL MODEL

The relaxation rate k of the excited state of the silica−RB NPs includes radiative and nonradiative parts.

$$k = k_r + k_{nr} \quad (3)$$

where k_r and k_{nr} denote the radiative and nonradiative decay rate constant, respectively. The quantum yield of rose bengal in 2-propanol is determined using the standard solution Rhodamine B in ethanol (quantum yield 0.97). The quantum yield of silica−RB NPs, Q^o, is obtained by comparing the fluorescence intensity of RB in 2-propanol. From the measured quantum yield (value 0.35) and emission lifetime (1.3 ns) of silica−RB NPs, we obtained the radiative and nonradiative rate constant to be 2.7×10^8 and 5×10^8 s^{-1}, respectively.

While the fluorophores are placed in the vicinity of GNP, their fluorescence decay curves are biexponential, indicating that the interaction mechanism of the metal NP−fluorophore system includes multiple pathways, distinct from that in silica−RB NPs. Upon photoexcitation, the fluorophores in the excited state can relax to the ground state via intrinsic nonradiative decay with the rate constant, k_{nr}, transfer energy to GNP, and induce a mirror dipole on the GNP. Both the excited fluorophores and the induced mirror dipole can radiate into the far field, with the rate constant denoted $k_{r,m}$. After the resonant modes in the nanoparticles are excited, they decay radiatively or nonradiatively.[39] When the excited fluorophores are coupled to the bright (dipolar) modes of GNPs, denoted as $k_{ET,Fluo\rightarrow GNP(bright)}$, the bright modes preferentially dissipate energy radiatively. The bright mode in nanoparticles can radiate with rate constant $k_{r,GNP}$, or transfer energy back to the fluorophores, $k_{ET,GNP(bright)\rightarrow Fluo}$. This would result in biexponential decay behavior in the emission of fluorophore. The excited fluorophores can also couple to the dark modes of GNPs and these dark modes dissipate energy nonradiatively; the rate constants for these processes are separately denoted as $k_{ET,Fluo\rightarrow GNP(dark)}$ and $k_{nr,GNP}$.

Overall, the kinetic model including these processes is proposed as depicted in Figure 6. Here we assume that the fraction of the dark modes undergoing energy transfer back to the fluorophore is negligible because other nonradiative processes are dominant. The intrinsic nonradiative decay k_{nr} of RB next to an Au@SiO_2 NP is assumed to be the same as that in silica−RB NPs because of the identical environment and attachment.

On the basis of this kinetic model and given the measured values of time constant τ_1 and τ_2 and the ratio of amplitudes A_1/A_2, we cannot obtain the value of each rate constant. However, a combination of rate constants can be calculated (details in the Supporting Information), the values of k_1

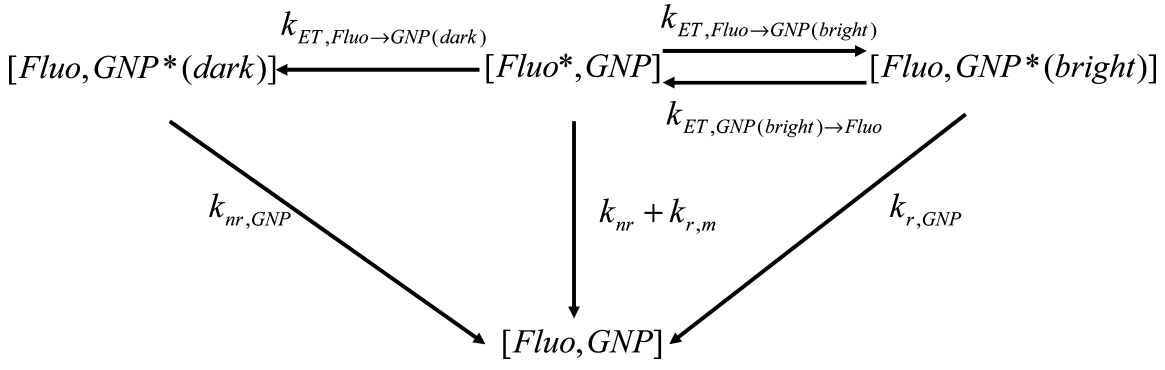

Figure 6. Kinetic model proposed for the energy transfer pathways of the excited Au@SiO_2−RB NPs. See the text for description of each pathway. Due to the small Stokes shift of fluorophore, the bright mode of the GNP may radiate into the far field, $k_{r,GNP}$, or energy may transfer to the fluorophore, $k_{ET,GNP(bright)\rightarrow Fluo}$.

DOI: 10.1021/acs.jpcc.5b08477
J. Phys. Chem. C 2015, 119, 26663−26671

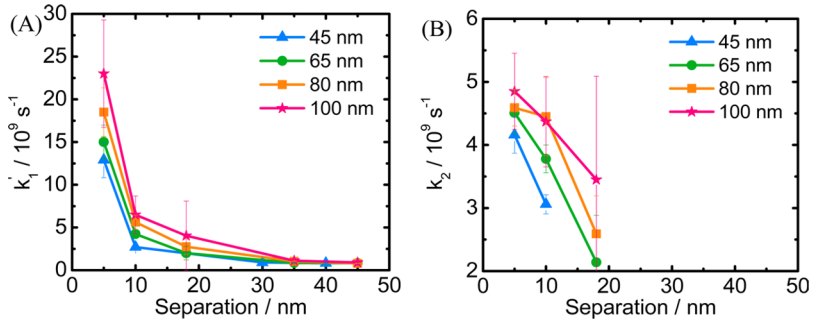

Figure 7. Rate constants k_1' and k_2 as a function of spacer thickness. Every rate constant was obtained through a series of calculations. As a result, the error bar is large, especially for small values of rate constants.

(defined as $k_1 = k_{r,m} + k_{ET,Fluo\rightarrow GNP(dark)} + k_{nr}$, for the processes of transfer to dark modes and decay of fluorophore) and k_2 (= $k_{ET,Fluo\rightarrow GNP(bright)} + k_{ET,GNP(bright)\rightarrow Fluo} + k_{r,GNP}$, for th processes of forward and backward transfer to bright modes and decay). Because k_{nr} is the intrinsic nonradiative decay rate constant of fluorophore and is invariant, k_1'(defined as $k_1 - k_{nr}$) is introduced to observe its distance and size dependence in MEF. k_1' and k_2 are plotted versus spacer thickness in Figure 7. For 100 nm GNPs, the range of k_1' is 4×10^8 to 2.3×10^{10} s^{-1}, and that of k_2 is 3.5×10^9 to 4.9×10^9 s^{-1}; both decrease with increasing spacer thickness but increase with the size of the NP. Because the polarizability of metal nanoparticles increases with size as a^3 (radius a), the induced mirror dipole on the GNP is proportional to the polarizability. Hence, $k_{r,m}$, which is mostly dominated by the induced mirror dipole, is expected to increase with the size of the NP. We calculated the values of $k_{r,m}$, which turns out to only slightly increase with size of NP, following the method reported by Guzatov et al.[40] For large GNPs with more dark modes, $k_{ET,fluo\rightarrow GNP(dark)}$ is expected to increase and should contribute the most to the increase of k_1' with size.

Case $k_{r,GNP} \gg k_{ET,GNP(bright)\rightarrow Fluo}$. To estimate the individual rate constants, we tried to simplify the kinetic model. If the bright modes of GNPs mostly radiate into the far field instead of transferring energy back to fluorophores, i.e., $k_{r,GNP} \gg k_{ET,GNP(bright)\rightarrow Fluo}$, the quantum yield of Au@SiO_2−RB NPs can be expressed as sum of radiation from the fluorophore Q_{Fluo} and the GNP Q_{GNP} (for detailed derivation see the Supporting Information)

$$Q = Q_{Fluo} + Q_{GNP} \cong \frac{\int_0^\infty k_{r,m}[\text{Fluo}^*, \text{GNP}]\, dt}{[\text{Fluo}^*, \text{GNP}]_0} + \frac{\int_0^\infty k_{r,GNP}[\text{Fluo}, \text{GNP}^*(\text{bright})]\, dt}{[\text{Fluo}^*, \text{GNP}]_0} \quad (4)$$

Using the detected fluorescence enhancement factor and the calculated excitation enhancement factor (I_{ex}/I_{ex}^0), the fluorescence quantum yield Q of Au@SiO_2−RB NPs can be calculated with the following equation.

$$\frac{I_{fluo}}{I_{fluo}^0} = \frac{I_{ex}}{I_{ex}^0}\frac{Q}{Q^0} \quad (5)$$

where I_{ex}/I_{ex}^0 is from the local electric field on the GNP defined as

$$\frac{I_{ex}}{I_{ex}^0} = \frac{|E_0 + E_p|^2}{|E_0|^2} \quad (6)$$

The E_0 and E_p are the electric field of the incident light wave and the local electric field of the metal nanoparticles, respectively. I_{ex}/I_{ex}^0 for GNPs of four diameters are calculated using the eq 6 and those given by Guzatov et al.,[40] and the values are displayed in Figure 8. Accordingly, I_{ex}/I_{ex}^0 decreases monotonically with the separation, and the greater GNPs render better enhancement in the excitation process.

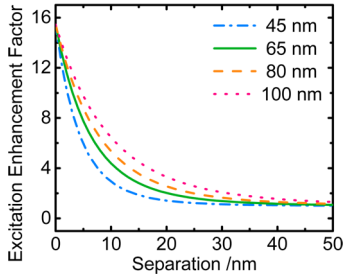

Figure 8. Calculated, averaged excitation enhancement factor for GNPs of four sizes as a function of separation from the surface of the GNP with an excitation wavelength of 532 nm.

Using the additional information on the quantum yield determined from eqs 4−6, we obtained the radiative decay rate constant of Au@SiO_2−RB NPs, $k_{r,m}$. The values of $k_{r,m}$ for 65 nm GNPs are 4.1×10^8, 1.1×10^8, and 1.7×10^8 s^{-1} for spacer thicknesses 5, 10, and 18 nm, respectively. Some of the calculated values are even less than the intrinsic radiative decay rate constant k_r of RB. Hence, those values are in conflict with the experimental facts that the fluorescence was enhanced. As a result, the assumption $k_{r,GNP} \gg k_{ET,GNP(bright)\rightarrow Fluo}$ fails to obtain correct experimental data; i.e., energy transfer from the bright modes of the GNPs to the fluorophores cannot be neglected.

Case $k_{ET,GNP(bright)\rightarrow Fluo} \gg k_{r,GNP}$. In this case, we assume that the bright modes of GNPs mostly transfer energy to the fluorophores, i.e., $k_{ET,GNP(bright)\rightarrow Fluo} \gg k_{r,GNP}$. This can be explained by the fact that the Stokes shift of RB is so small that strong interaction exists between the GNPs and the fluorophore. In this case, the quantum yield of Au@SiO_2−RB NPs is estimated as

$$Q \approx \frac{\int_0^\infty k_{r,m}[\text{Fluo}^*, \text{GNP}]\, dt}{[\text{Fluo}^*, \text{GNP}]_0} = \frac{k_{r,m}}{b' - a'}\left[\frac{c' - a'}{a'} - \frac{c' - b'}{b'}\right] \quad (7)$$

DOI: 10.1021/acs.jpcc.5b08477
J. Phys. Chem. C 2015, 119, 26663−26671

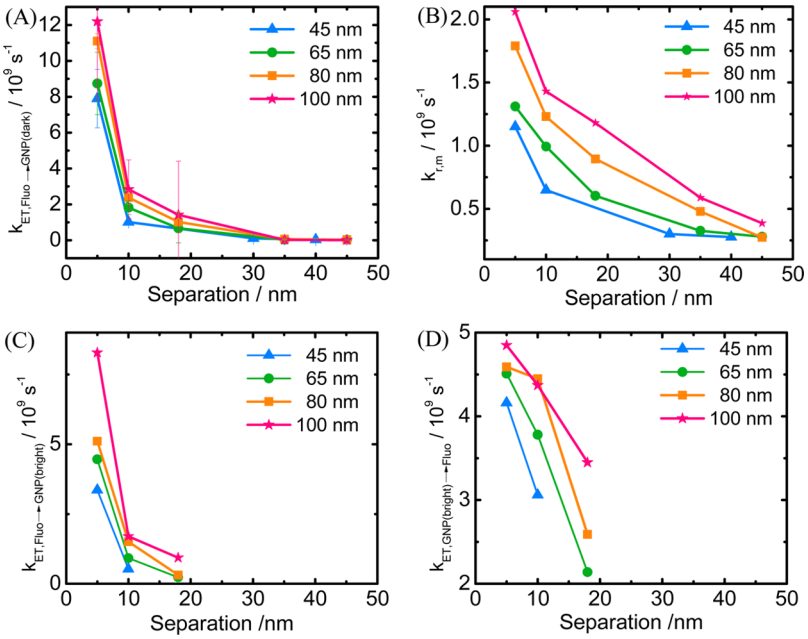

Figure 9. Plots of $k_{ET,Fluo\rightarrow GNP(dark)}$, $k_{r,m}$, $k_{ET,Fluo\rightarrow GNP(bright)}$, and $k_{ET,GNP(bright)\rightarrow Fluo}$ vs size of GNP and separation of silica spacer. The rate constants are calcualted; hence, the error bar is large, especially for small values of rate constant. Only the error bar ($\pm\sigma$) of $k_{ET,Fluo\rightarrow GNP(dark)}$ is shown.

where $a' + b' = k_{nr} + k_{r,m} + k_{ET,Fluo\rightarrow GNP(bright)} + k_{ET,Fluo\rightarrow GNP(dark)} + k_{ET,GNP(bright)\rightarrow Fluo}$, $a' \times b' = (k_{nr} + k_{r,m} + k_{ET,Fluo\rightarrow GNP(dark)}) \times k_{ET,GNP(bright)\rightarrow Fluo}$, and $c' = k_{ET,GNP(bright)\rightarrow Fluo}$ (more details in Supporting Information.) According to calculated excitation enhancement, the quantum yield of silica−RB NPs, and fluorescence enhancement, we can obtain the quantum yield of Au@SiO_2−RB using eq 5. The value of $k_{r,m}$ is thus obtained by means of the experimental determined Q.

Figure 9 shows the size and distance effects on $k_{r,m}$, $k_{ET,Fluo\rightarrow GNP(dark)}$, $k_{ET,Fluo\rightarrow GNP(bright)}$, and $k_{ET,GNP(bright)\rightarrow Fluo}$. The value of $k_{ET,Fluo\rightarrow GNP(dark)}$ is greater for larger GNPs and displays a sharp decrease as separation. For 100 nm GNPs, $k_{ET,Fluo\rightarrow GNP(dark)}$ ranges from 2.7×10^7 to 1.2×10^{10} s^{-1}, and its amplitude is dominant at short separations. $k_{ET,GNP(bright)\rightarrow Fluo}$ ranges from 3.5×10^9 to 4.9×10^9 s^{-1} for separation of 18 to 5 nm. Because the radiation of the bright modes of GNPs is believed to be related to the scattering efficiency of the Au@SiO_2 NPs, both $k_{ET,Fluo\rightarrow GNP(bright)}$ and $k_{ET,GNP(bright)\rightarrow Fluo}$ are found to increase with GNP size. When the separation is large, the interaction becomes weak, leading to significant decreases in those rate constants. With separation of greater than 30 nm, the interaction is so weak that the time-resolved fluorescence curves show single exponential decay behavior, which means negligible $k_{ET,Fluo\rightarrow GNP(bright)}$ and $k_{ET,GNP(bright)\rightarrow Fluo}$.

The mirror dipole on the metal nanoparticle induced by the excited fluorophore is added to the original electric field, which in turn interacts with the molecular dipole of the fluorophore.[41] The radiative decay rate is determined by the total dipole moment of the fluorophore−plasmonic system. Accordingly, the enhancement factor of the radiative decay rate is then written as

$$\frac{k_{r,m}}{k_r} = \frac{|d_0 + \delta d|^2}{|d_0|^2} \quad (12)$$

where d_0 is the molecule dipole moment and δd is the induced dipole moment. The calculated enhancement factor of the radiative decay rate using this equation (more in the Supporting Information) and the factor based on the experimental measurement and the kinetic model under case $k_{ET,GNP(bright)\rightarrow Fluo} \gg k_{r,GNP}$ are displayed in Figure 10. These

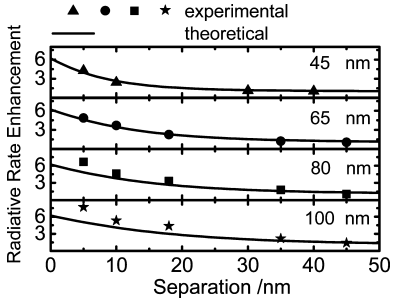

Figure 10. Theoretical (solid line) and experimental results for averaged radiative decay rate enhancement factor. The sizes of the gold nanoparticles are 45 (triangle), 65 (circle), 80 (square), and 100 nm (star). The experimental radiative decay rate of Au@SiO_2−RB NPs is obtained using eq 7. The experimental radiative decay rate enhancement factor is the ratio radiative decay rate of Au@SiO_2−RB NPs and the intrinsic radiative decay rate of silica−RB NPs (2.7×10^8). The theoretical radiative decay rate enhancement factor is calculated using eq 12.

values agree for small NPs. Some discrepancies arise for large GNPs. This might be because the limit $k_{ET,GNP(bright)\rightarrow Fluo} \gg k_{r,GNP}$ becomes failure under these conditions; i.e., the contribution of radiation from the bright modes of the GNPs ($k_{r,GNP}$) cannot be ignored.

5. DISCUSSION

If we plot the logarithm of $k_{ET,Fluo\rightarrow GNP(dark)}$ and $k_{ET,Fluo\rightarrow GNP(bright)}$ vs thickness of the silica spacer d (as shown in Figures S9 and S10), we obtain a slope $n \approx 2.5$; the rate constant is $\propto d^{-n}$, an exponent smaller than $n = 4$, as expected using the theory of NSET, not to mention the $n = 6$ in FRET.

DOI: 10.1021/acs.jpcc.5b08477
J. Phys. Chem. C 2015, 119, 26663−26671

The GNPs used in the present work were large. However, a similar discrepancy has also been reported by Chhabra et al. for 10 nm nanoparticles.[26] Hence, the interaction of fluorophore to NPs differs from the expected by those theories.

According to the previous studies,[42,43] when fluorophores are close to GNPs, the excited fluorophores have faster radiative decay rates and additional energy transfers to the GNPs, leading to quenching. On the basis of this mechanism, the emission curves of Au@SiO_2−RB NPs for short separations should display single exponential behavior with fast decay. In the present work, it is reasonable to infer that the excited fluorophores transfer energy to the bright modes of GNPs, and the bright modes may either radiate into the far field or transfer energy back to the fluorophores to explain the biexponential behavior in the emission decay curves. According to our data analysis, energy transfer from the bright modes of GNPs to fluorophores cannot be neglected at short distances. For small GNPs, because the scattering cross section is relatively small, the radiation of the bright mode can be ignored. At very small separation, the energy transfer from fluorophores to the dark modes of GNPs, which leads to quenching is overwhelmingly dominant. Therefore, the fluorescence enhancement is mostly attributed to excitation enhancement instead of the radiative decay enhancement. At large separation, the emission decay curves of Au@SiO_2−RB NPs become single exponential decay, indicating negligible energy transfer and radiation from the bright modes of GNPs.

6. CONCLUSION

Au@SiO_2 NPs are used to systematically study the interaction between gold nanoparticles and fluorophore rose bengal (RB) via steady-state and time-resolved fluorescence spectroscopy. Both the fluorescence intensity and lifetime are found to exhibit distance and size dependence. When fluorophores are placed in the vicinity of metal nanoparticles, both radiative decay rate and energy transfer rate to GNPs decrease with distance. Radiation and energy transfer to fluorophores from bright modes of GNPs and nonradiation from dark modes of GNP are also observed to decrease with distance; the later process is dominant at shorter distance. Our experimental data show the maximal fluorescence enhancement at varied sizes of NPs at around 10 nm separation of silica spacer; this agrees with the results of other groups at 3−17 nm.[44−47] Fluorescence enhancement and all relaxation rates involved in the metal-fluorophore system were also observed to increase with the size of the GNPs.

■ ASSOCIATED CONTENT

Supporting Information

The Supporting Information is available free of charge on the ACS Publications website at DOI: 10.1021/acs.jpcc.5b08477.

TEM images of Au@SiO_2 NPs, surface plasmon resonance band of Au@SiO_2 NPs, emission spectra of Au@SiO_2−RB, time-resolved decay profiles, quantum yield of Au@SiO_2−RB, log plots of rate constant vs silica shell thickness, tables of silica shell thickness, surface plasmon band centers of Au@SiO_2 NPs, and kinetic model analysis; discussion of excitation and radiative decay rate enhancement factor (PDF)

■ AUTHOR INFORMATION

Corresponding Author

*E-mail: icchen@mx.nthu.edu.tw.

Notes

The authors declare no competing financial interest.

■ ACKNOWLEDGMENTS

We are grateful for the support of National Tsing Hua University, under project "Frontier Research Center on Fundamental and Applied Sciences of Matter", and the Ministry of Science and Technology of Republic of China.

■ REFERENCES

(1) Cubeddu, R.; Comelli, D.; Andrea, C. D.; Taroni, P.; Valentini, G. Time-Resolved Fluorescence Imaging in Biology and Medicine. *J. Phys. D: Appl. Phys.* **2002**, *35*, 65−76.

(2) Berezin, M. Y.; Achilefu, S. Fluorescence Lifetime Measurements and Biological Imaging. *Chem. Rev.* **2010**, *110*, 2641−2684.

(3) Geng, J. L.; Liang, J.; Wang, Y. S.; Gurzadyan, G. G.; Liu, B. Metal-Enhanced Fluorescence of Conjugated Polyelectrolytes with Self-Assembled Silver Nanoparticle Platforms. *J. Phys. Chem. B* **2011**, *115*, 3281−3288.

(4) Lakowicz, J. R. Radiative Decay Engineering: Biophysical and Biomedical Applications. *Anal. Biochem.* **2001**, *298*, 1−24.

(5) Klimov, V. V.; Ducloy, M.; Letokhov, V. S. Spontaneous Emission of an Atom in the Presence of Nanobodies. *Quantum Electron.* **2001**, *31*, 569−586.

(6) Fort, E.; Gresillon, S. Surface Enhanced Fluorescence. *J. Phys. D: Appl. Phys.* **2008**, *41*, 013001.

(7) Zhang, J.; Fu, Y.; Chowdhury, M. H.; Lakowicz, J. R. Metal-Enhanced Single-Molecule Fluorescence on Silver Particle Monomer and Dimer: Coupling Effect Between Metal Particles. *Nano Lett.* **2007**, *7*, 2101−2107.

(8) Schneider, G.; Decher, G.; Nerambourg, N.; Praho, R.; Werts, M. H. V.; Blanchard-Desce, M. Distance-Dependent Fluorescence Quenching on Gold Nanoparticles Ensheathed with Layer-by-Layer Assembled Polyelectrolytes. *Nano Lett.* **2006**, *6*, 530−536.

(9) Dulkeith, E.; Morteani, A. C.; Niedereichholz, T.; Klar, T. A.; Feldmann, J.; Levi, S. A.; van Veggel, F. C. J. M.; Reinhoudt, D. N.; Moller, M.; Gittins, D. I. Fluorescence Quenching of Dye Molecules near Gold Nanoparticles: Radiative and Nonradiative Effects. *Phys. Rev. Lett.* **2002**, *89*, 203002.

(10) Ray, K.; Badugu, R.; Lakowicz, J. R. Distance-Dependent Metal-Enhanced Fluorescence from Langmuir-Blodgett Monolayers of Alkyl-Nbd Derivatives on Silver Island Films. *Langmuir* **2006**, *22*, 8374−8378.

(11) Ray, K.; Badugu, R.; Lakowicz, J. R. Sulforhodamine Adsorbed Langmuir-Blodgett Layers on Silver Island Films: Effect of Probe Distance on the Metal-Enhanced Fluorescence. *J. Phys. Chem. C* **2007**, *111*, 7091−7097.

(12) Bharadwaj, P.; Novotny, L. Spectral Dependence of Single Molecule Fluorescence Enhancement. *Opt. Express* **2007**, *15*, 14266−14274.

(13) Kang, K. A.; Wang, J. T.; Jasinski, J. B.; Achilefu, S. Fluorescence Manipulation by Gold Nanoparticles: From Complete Quenching to Extensive Enhancement. *J. Nanobiotechnol.* **2011**, *9*, 16.

(14) Aslan, K.; Malyn, S. N.; Zhang, Y. X.; Geddes, C. D. Conversion of Just-Continuous Metallic Films to Large Particulate Substrates for Metal-Enhanced Fluorescence. *J. Appl. Phys.* **2008**, *103*, 084307.

(15) Aslan, K.; Geddes, C. D. Metal-Enhanced Fluorescence: Progress Towards a Unified Plasmon-Fluorophore Description. In *Metal-Enhanced Fluorescence*; Geddes, C. D., Ed.; John Wiley & Sons, Inc: Hoboken, NJ, 2010; pp 1−23.

(16) Zhang, Y.; Dragan, A.; Geddes, C. D. Wavelength Dependence of Metal-Enhanced Fluorescence. *J. Phys. Chem. C* **2009**, *113*, 12095−12100.

DOI: 10.1021/acs.jpcc.5b08477
J. Phys. Chem. C 2015, 119, 26663−26671

(17) Xie, F.; Baker, M. S.; Goldys, E. M. Enhanced Fluorescence Detection on Homogeneous Gold Colloid Self-Assembled Monolayer Substrates. *Chem. Mater.* **2008**, *20*, 1788−1797.
(18) Sun, G.; Khurgin, J. B.; Soref, R. A. Practical Enhancement of Photoluminescence by Metal Nanoparticles. *Appl. Phys. Lett.* **2009**, *94*, 101103.
(19) Reineck, P.; Gomez, D.; Ng, S. H.; Karg, M.; Bell, T.; Mulvaney, P.; Bach, U. Distance and Wavelength Dependent Quenching of Molecular Fluorescence by Au@SiO_2 Core-Shell Nanoparticles. *ACS Nano* **2013**, *7*, 6636−6648.
(20) Bhowmick, S.; Saini, S.; Shenoy, V. B.; Bagchi, B. Resonance Energy Transfer from a Fluorescent Dye to a Metal Nanoparticle. *J. Chem. Phys.* **2006**, *125*, 181102.
(21) Saini, S.; Bhowmick, S.; Shenoy, V. B.; Bagchi, B. Rate of Excitation Energy Transfer Between Fluorescent Dyes and Nanoparticles. *J. Photochem. Photobiol., A* **2007**, *190*, 335−341.
(22) Yun, C. S.; Javier, A.; Jennings, T.; Fisher, M.; Hira, S.; Peterson, S.; Hopkins, B.; Reich, N. O.; Strouse, G. F. Nanometal Surface Energy Transfer in Optical Rulers, Breaking the Fret Barrier. *J. Am. Chem. Soc.* **2005**, *127*, 3115−3119.
(23) Chance, R. R.; Prock, A.; Silbey, R. Molecular Fluorescence and Energy Transfer Near Interfaces. In *Adchp*, Prigogine, I., Rice, S. A., Eds.; John Wiley & Sons, Inc.: Hoboken, NJ, 1978; Vol. 37, pp 1−65.
(24) Sen, T.; Sadhu, S.; Patra, A. Surface Energy Transfer from Rhodamine 6g to Gold Nanoparticles: A Spectroscopic Ruler. *Appl. Phys. Lett.* **2007**, *91*, 043104.
(25) Jennings, T. L.; Singh, M. P.; Strouse, G. F. Fluorescent Lifetime Quenching near D = 1.5 Nm Gold Nanoparticles: Probing Nset Validity. *J. Am. Chem. Soc.* **2006**, *128*, 5462−5467.
(26) Chhabra, R.; Sharma, J.; Wang, H. N.; Zou, S. L.; Lin, S.; Yan, H.; Lindsay, S.; Liu, Y. Distance-Dependent Interactions Between Gold Nanoparticles and Fuorescent Molecules with DNA as Tunable Spacers. *Nanotechnology* **2009**, *20*, 485201.
(27) Griffin, J.; Singh, A. K.; Senapati, D.; Rhodes, P.; Mitchell, K.; Robinson, B.; Yu, E.; Ray, P. C. Size- and Distance-Dependent Nanoparticle Surface-Energy Transfer (NEST) Method for Selective Sensing of Hepatitis C Virus Rna. *Chem. - Eur. J.* **2009**, *15*, 342−351.
(28) Acuna, G. P.; Bucher, M.; Stein, I. H.; Steinhaurer, C.; Kuzyk, A.; Holzmeister, P.; Schreiber, R.; Moroz, A.; Stefani, F. D.; Liedl, T. Distance Dependence of Single-Fluorophore Quenching by Gold Nanoparticles Studied on DNA Origami. *ACS Nano* **2012**, *6*, 3189−3195.
(29) Bardhan, R.; Grady, N. K.; Cole, J. R.; Joshi, A.; Halas, N. J. Fluorescence Enhancement by Au Nanostructures: Nanoshells and Nanorods. *ACS Nano* **2009**, *3*, 744−752.
(30) Ray, K.; Badugu, R.; Lakowicz, J. R. Polyelectrolyte Layer-by-Layer Assembly to Control the Distance between Fluorophores and Plasmonic Nanostructures. *Chem. Mater.* **2007**, *19*, 5902−5909.
(31) Bardhan, R.; Grady, N. K.; Halas, N. J. Nanoscale Control of Near-Infrared Fluorescence Enhancement Using Au Nanoshells. *Small* **2008**, *4*, 1716−1722.
(32) Yang, Z.; Ni, W. H.; Kou, X. S.; Zhang, S. Z.; Sun, Z. H.; Sun, L. D.; Wang, J. F.; Yan, C. H. Incorporation of Gold Nanorods and Their Enhancement of Fluorescence in Mesostructured Silica Thin Films. *J. Phys. Chem. C* **2008**, *112*, 18895−18903.
(33) Liu, S. Y.; Huang, L.; Li, J. F.; Wang, C.; Li, Q.; Xu, H. X.; Guo, H. L.; Meng, Z. M.; Shi, Z.; Li, Z. Y. Simultaneous Excitation and Emission Enhancement of Fluorescence Assisted by Double Plasmon Modes of Gold Nanorods. *J. Phys. Chem. C* **2013**, *117*, 10636−10642.
(34) Yuan, H. F.; Khatua, S.; Zijlstra, P.; Yorulmaz, M.; Orrit, M. Thousand-Fold Enhancement of Single-Molecule Fluorescence Near a Single Gold Nanorod. *Angew. Chem., Int. Ed.* **2013**, *52*, 1217−1221.
(35) Pastoriza-Santos, I.; Perez-Juste, J.; Liz-Marzan, L. M. Silica-Coating and Hydrophobation of Ctab-Stabilized Gold Nanorods. *Chem. Mater.* **2006**, *18*, 2465−2467.
(36) Rodriguez-Fernandez, J.; Pastoriza-Santos, I.; Perez-Juste, J.; de Abajo, F. J. G.; Liz-Marzan, L. M. The Effect of Silica Coating on the Optical Response of Sub-Micrometer Gold Spheres. *J. Phys. Chem. C* **2007**, *111*, 13361−13366.
(37) Guo, Y. Y.; Rogelj, S.; Zhang, P. Rose Bengal-Decorated Silica Nanoparticles as Photosensitizers for Inactivation of Gram-Positive Bacteria. *Nanotechnology* **2010**, *21*, 065102.
(38) Buehler, C.; Dong, C. Y.; So, P. T. C.; French, T.; Gratton, E. Time-Resolved Polarization Imaging by Pump-Probe (Stimulated Emission) Fluorescence Microscopy. *Biophys. J.* **2000**, *79*, 536−549.
(39) Sun, G.; Khurgin, J. B.; Tsai, D. P. Comparative Analysis of Photoluminescence and Raman Enhancement by Metal Nanoparticles. *Opt. Lett.* **2012**, *37*, 1583−1585.
(40) Guzatov, D. V.; Vaschenko, S. V.; Stankevich, V. V.; Lunevich, A. Y.; Glukhov, Y. F.; Gaponenko, S. V. Plasmonic Enhancement of Molecular Fluorescence near Silver Nanoparticles: Theory, Modeling, and Experiment. *J. Phys. Chem. C* **2012**, *116*, 10723−10733.
(41) Klar, T. A.; Feldmann, J. Fluorophore−Metal Nanoparticle Interactions and Their Applications in Biosensing. *Complex-Shaped Metal Nanoparticles*; Wiley-VCH Verlag GmbH & Co. KGaA: Weinheim, 2012; pp 395−427.
(42) Muskens, O. L.; Giannini, V.; Sanchez-Gil, J. A.; Rivas, J. G. Strong Enhancement of the Radiative Decay Rate of Emitters by Single Plasmonic Nanoantennas. *Nano Lett.* **2007**, *7*, 2871−2875.
(43) Fu, Y.; Zhang, J.; Lakowicz, J. R. Silver-Enhanced Fluorescence Emission of Single Quantum Dot Nanocomposites. *Chem. Commun.* **2009**, 313−315.
(44) Wang, J. T.; Moore, J.; Laulhe, S.; Nantz, M.; Achilefu, S.; Kang, K. A. Fluorophore-Gold Nanoparticle Complex for Sensitive Optical Biosensing and Imaging. *Nanotechnology* **2012**, *23*, 095501.
(45) Abadeer, N. S.; Brennan, M. R.; Wilson, W. L.; Murphy, C. J. Distance and Plasmon Wavelength Dependent Fluorescence of Molecules Bound to Silica-Coated Gold Nanorods. *ACS Nano* **2014**, *8*, 8392−8406.
(46) Anger, P.; Bharadwaj, P.; Novotny, L. Enhancement and Quenching of Single-Molecule Fluorescence. *Phys. Rev. Lett.* **2006**, *96*, 113002.
(47) Fu, B.; Flynn, J. D.; Isaacoff, B. P.; Rowland, D. J.; Biteen, J. S. Super-Resolving the Distance-Dependent Plasmon-Enhanced Fluorescence of Single Dye and Fluorescent Protein Molecules. *J. Phys. Chem. C* **2015**, *119*, 19350−19358.

DOI: 10.1021/acs.jpcc.5b08477
J. Phys. Chem. C 2015, 119, 26663−26671